J Math Imaging Vis (2011) 41:210–221
DOI 10.1007/s10851-011-0271-5

General Adaptive Neighborhood-Based Pretopological Image Filtering

Johan Debayle · Jean-Charles Pinoli

Published online: 10 March 2011

Abstract This paper introduces pretopological image filtering in the context of the General Adaptive Neighborhood Image Processing (GANIP) approach. Pretopological filters act on gray level image while satisfying some topological properties. The GANIP approach enables to get an image representation and mathematical structure for adaptive image processing and analysis. Then, the combination of pretopology and GANIP leads to efficient image operators. They enable to process images while preserving region structures without damaging image transitions. More precisely, GAN-based pretopological filters and GAN-based viscous pretopological filters are proposed in this paper. The viscous notion enables to adjust the filtering activity to the image gray levels. These adaptive filters are evaluated through several experiments highlighting their efficiency with respect to the classical operators. They are practically applied in both the biomedical and material application areas for image restoration, image background subtraction and image enhancement.

Keywords Adaptive image processing · General adaptive neighborhoods · Pretopology · Viscous filtering

1 Introduction

The framework entitled General Adaptive Neighborhood Image Processing (GANIP) has been introduced [11, 12] in order to propose an original image representation and mathematical structure for adaptive image processing and analysis. For each point of the image spatial support, a set of adaptive local neighborhoods (GANs) is introduced. They can be used as operational windows for setting up adaptive image filters such as proposed in [8, 9, 13, 32].

These specific neighborhoods are here studied from a topological (more precisely pretopological) point of view [5]. Indeed, they enable to define generalized topologies [5, 37, 40], i.e. based on less axioms than classical topologies [5, 6, 35]. For example, several pretopological structures (i.e. satisfying specific axioms) have been studied [23, 37, 40] and particularly applied for image processing [1, 2, 4, 24, 28, 29, 36]. Nevertheless, the resulting image transformations are generally not adaptive with respect to the spatial structures. Indeed, the pretopological adherency of a point is restricted to points within a fixed-shape and fixed-size analyzing (operational) window.

In this paper, pretopological structures are proposed in accordance with the GANIP framework. In this way, efficient adaptive image processing filters are defined, studied and compared to classical operators. More precisely, GAN-based pretopological filters and GAN-based viscous pretopological filters are proposed in this paper. The viscous notion [25, 44] enables to adjust the filtering activity to the image gray levels. The theoretical advantages of the proposed GAN-based pretopological (viscous) filters are practically highlighted on real application examples for image restoration, image background subtraction and image enhancement.

The paper first outlines the concept and definitions of generalized topologies (Sect. 2). Then, the GANIP approach is briefly exposed in Sect. 3. The definition and properties of the GAN-based pretopologies are proposed and studied in Sect. 4. Thus, GAN-based pretopological filters (Sect. 5)

J. Debayle (✉) · J.-C. Pinoli
Ecole Nationale Supérieure des Mines, CIS-LPMG, CNRS,
158, cours Fauriel, 42023 Saint-Etienne Cedex 2, France
e-mail: debayle@emse.fr

J.-C. Pinoli
e-mail: pinoli@emse.fr

and GAN-based viscous pretopological filters (Sect. 6) are defined and are performed on real application examples (Sect. 7). Finally, the conclusion and perspectives of the proposed approach are discussed in Sect. 8.

2 Generalized Topologies

In this section, several theoretical notions of generalized topologies are callbacked. These generalized topologies are defined with less axioms than classical topologies which have been largely used in image processing and analysis from long years ago up to now [3, 7, 18–22, 35]. Nevertheless, some axioms could be not consistent with the formulation of proximity/distance in image analysis [42]. More generally, several generalized topological structures have been proposed in the literature [2, 5, 23, 37–40]. Some of those structures could not be metrized but only pseudometrized, i.e. using a weak metric [37, 41].

From a mathematical point of view, each generalized topology could be introduced starting from a pseudoclosure function.

2.1 Pseudoclosure Function

For a 2-dimensional set $D \subseteq \mathbb{R}^2$, the pseudoclosure on $\mathcal{P}(D) = \{A; A \subseteq D\}$ is a function:

$$\mathrm{clo} : \begin{cases} \mathcal{P}(D) \to \mathcal{P}(D) \\ A \mapsto \mathrm{clo}(A) \end{cases} \tag{1}$$

satisfying the following properties:

- $\mathrm{clo}(\emptyset) = \emptyset$
- $\forall A \in \mathcal{P}(D)\ A \subseteq \mathrm{clo}(A)$

2.2 Pseudointerior, Neighborhood and Convergent Functions

The dual of the pseudoclosure function is the pseudointerior function defined by:

$$\mathrm{int} : \begin{cases} \mathcal{P}(D) \to \mathcal{P}(D) \\ A \mapsto \mathrm{int}(A) = {}^c(\mathrm{clo}({}^c A)) \end{cases} \tag{2}$$

where ${}^c Z = D \backslash Z$.

The neighborhood function assigns to each $x \in D$ the collections of its neighborhoods:

$$\mathcal{N}\mathrm{eigh} : \begin{cases} D \to \mathcal{P}(\mathcal{P}(D)) \\ x \mapsto \{N \in \mathcal{P}(D) \mid x \in \mathrm{int}(N)\} \end{cases} \tag{3}$$

The convergent function assigns to each $x \in D$ the collections of its convergents:

$$\mathcal{C}\mathrm{onv} : \begin{cases} D \to \mathcal{P}(\mathcal{P}(D)) \\ x \mapsto \{Q \in \mathcal{P}(D) \mid x \in \mathrm{clo}(Q)\} \end{cases} \tag{4}$$

2.3 Closure and Interior Functions

- $\forall A \in \mathcal{P}(D)\ A$ is close iff $\mathrm{clo}(A) = A$
- $\forall A \in \mathcal{P}(D)\ A$ is open iff $\mathrm{int}(A) = A$

In this way, the closure and interior notions could be introduced.

The closure function is defined as:

$$\overline{\mathrm{clo}} : \begin{cases} \mathcal{P}(D) \to \mathcal{P}(D) \\ A \mapsto \bigcap\{B \in \mathcal{P}(D) \mid \mathrm{clo}(B) = B, B \supseteq A\} \end{cases} \tag{5}$$

The interior function is the dual function:

$$\overset{\circ}{\mathrm{int}} : \begin{cases} \mathcal{P}(D) \to \mathcal{P}(D) \\ A \mapsto \bigcup\{B \in \mathcal{P}(D) \mid \mathrm{int}(B) = B, B \subseteq A\} \end{cases} \tag{6}$$

Note that $\overset{\circ}{\mathrm{int}}(A) = {}^c(\overline{\mathrm{clo}}({}^c A))$.

2.4 Axioms for Pseudoclosure Functions

Let (D, clo) be a generalized topological space and consider the following properties of the pseudoclosure function for all $A, B \in \mathcal{P}(D)$.

- (K0) $\mathrm{clo}(\emptyset) = \emptyset$
- (K1) $A \subseteq B \Rightarrow \mathrm{clo}(A) \subseteq \mathrm{clo}(B)$ (isotonic)
- (K2) $A \subseteq \mathrm{clo}(A)$ (expanding)
- (K3) $\mathrm{clo}(A \cup B) \subseteq \mathrm{clo}(A) \cup \mathrm{clo}(B)$ (sub-additive)
- (K4) $\mathrm{clo}(\mathrm{clo}(A)) = \mathrm{clo}(A)$ (idempotent)

These properties lead to different kinds of generalized topologies (see Table 1) up to the classical topology. In addition to these "pretopological axioms", few properties could be inferred from the previous ones:

- (K′0) $\exists A | x \notin \mathrm{clo}(A)$
- (KA) $\mathrm{clo}(D) = D$
- (KB) $A \cup B = D \Rightarrow \mathrm{clo}(A) \cup \mathrm{clo}(B) = D$

with the following relationships:

1. (K0) $\Rightarrow$ (K0′)
2. (K2), (K3) $\Rightarrow$ (KB)
3. (K0) + (KB) $\Rightarrow$ (KA)

2.5 Axioms and Generalized Topologies

The axioms (K_i) stated in the previous paragraph define several generalized topological spaces on D.

The following section callbacks the notion of General Adaptive Neighborhoods (GANs). These specific neighborhoods will be used for defining different pseudoclosure functions and consequently different generalized topologies on the spatial support of the images.

Table 1 Generalized topological axioms for pseudoclosure functions

Generalized topologies	(K0): $\text{clo}(\emptyset) = \emptyset$	(K1): $A \subseteq B \Rightarrow \text{clo}(A) \subseteq \text{clo}(B)$	(K2): $A \subseteq \text{clo}(A)$	(K3): $\text{clo}(A \cup B) \subseteq \text{clo}(A) \cup \text{clo}(B)$	(K4): $\text{clo}(\text{clo}(A)) = \text{clo}(A)$
Extended topology	•	•			
Brissaud space	•		•		
Neighborhood space	•	•	•		
Closure space	•	•	•		•
Smyth space	•	•		•	
Pretopology	•	•	•	•	
Topology	•	•	•	•	•

3 General Adaptive Neighborhoods (GANs)

This paper deals with 2D intensity images, that is to say image mappings defined on a spatial support D in the Euclidean space $\mathbb{R}^2$ and valued into a gray level range, which is a real numbers interval. The General Adaptive Neighborhood paradigm has been introduced in order to propose an original image representation for adaptive processing and analysis. The central idea is the notion of adaptivity which is simultaneously associated to the analyzing scales, the spatial structures and the intensity values of the image to be addressed.

In the so-called General Adaptive Neighborhood Image Processing (GANIP) approach [10–12], a set of General Adaptive Neighborhoods (GANs set) is identified about each point in the image to be analyzed. A GAN is a subset of the spatial support constituted by connected points whose measurement values, in relation to a selected criterion (such as luminance, contrast, thickness, ...), fit within a specified homogeneity tolerance. These GANs are used as adaptive windows for image transformations or quantitative image analysis.

The space of *image* (resp. *criterion*) *mappings*, defined on the spatial support D and valued in a real numbers interval $\tilde{E}$ (resp. E), is represented in a General Linear Image Processing (GLIP) framework, denoted $\mathcal{I}$ (resp. $\mathcal{C}$). The GLIP framework $\mathcal{I}$ (resp. $\mathcal{C}$) is then supplied with an ordered vectorial structure, using the formal vector addition $\tilde{\oplus}$ (resp. $\oplus$), the formal scalar multiplication $\tilde{\otimes}$ (resp. $\otimes$) and the classical total order relation $\geq$ defined directly from those of real numbers:

$$\forall (f,g) \in \mathcal{I}^2 \text{ or } \mathcal{C}^2 \quad f \geq g \Leftrightarrow (\forall x \in D \; f(x) \geq g(x)) \tag{7}$$

The most frequently used framework is the *Classical Linear Image Processing* framework where the vector addition and the vector multiplication are the usual $+$ and $\times$ operations, respectively. Additional frameworks have been developed. For example, the *Logarithmic Image Processing* (LIP) framework of intensity images $(f, g, \ldots)$ has been introduced [16, 17] with its vector addition $\mathbin{\text{⟑}}$, its vector subtraction $\mathbin{\text{⟇}}$ and its scalar multiplication $\mathbin{\text{⟁}}$ defined respectively as following:

$$f \mathbin{\text{⟑}} g = f + g - \frac{fg}{M} \tag{8}$$

$$f \mathbin{\text{⟇}} g = M\left(\frac{f-g}{M-g}\right) \tag{9}$$

$$\alpha \mathbin{\text{⟁}} f = M - M\left(1 - \frac{f}{M}\right)^{\alpha}, \quad \alpha \in \mathbb{R} \tag{10}$$

where $M \in \mathbb{R}$ denotes the upper bound of the range where intensity images are digitized and stored.

The LIP framework has been proved to be consistent with the transmittance image formation model, the multiplicative reflectance image formation model, the multiplicative transmittance image formation model, and with several laws and characteristics of human brightness perception [30, 31].

There exists several GANs sets, whose each collection satisfies specific properties [11]. This paper callbacks the weak and strong GANs, denoted $V^h_{m_{\bigcirc}}(x)$ and $N^h_{m_{\bigcirc}}(x)$, respectively.

3.1 Weak GANs

For each point $x \in D$ and for an image $f \in \mathcal{I}$, the GANs $V^h_{m_{\bigcirc}}(x)$ are included as subsets in D. They are built upon a *criterion mapping* $h \in \mathcal{C}$ (based on a local measurement such as luminance, contrast, thickness, ... related to f), in relation with an *homogeneity tolerance* $m_{\bigcirc}$ belonging to the positive intensity value range $E^{\oplus}$. More precisely, $V^h_{m_{\bigcirc}}(x)$ is a subset of D which fulfills two conditions:

1. its points have a measurement value close to that of the point x: $\forall y \in V^h_{m_{\bigcirc}}(x) \; |h(y) \ominus h(x)|_{\bigcirc} \leq m_{\bigcirc}$, where $\ominus$ and $|.|_{\bigcirc}$ denote the considered GLIP subtraction and GLIP modulus, respectively,
2. the set is path-connected (with the usual Euclidean topology on $D \subseteq \mathbb{R}^2$).

The weak GANs are thus defined as following:

$$\forall (m_{\bigcirc}, h, x) \in E^{\oplus} \times \mathcal{C} \times D$$
$$V^h_{m_{\bigcirc}}(x) = C_{h^{-1}([h(x) \ominus m_{\bigcirc}, h(x) \oplus m_{\bigcirc}])}(x) \tag{11}$$

where $C_X(x)$ denotes the path-connected component (with the usual Euclidean topology on $D \subseteq \mathbb{R}^2$) of $X \subseteq D$ containing $x \in D$.

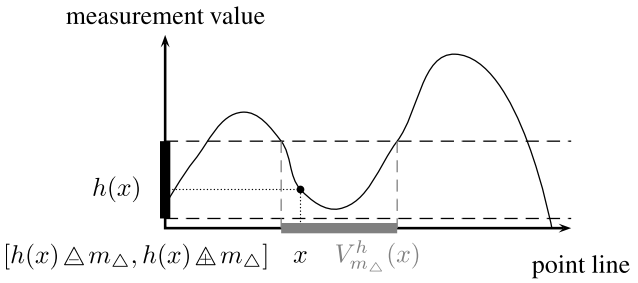

Fig. 1 One-dimensional computation of an adaptive neighborhood set $V^h_{m_{\triangle}}(x)$ in the LIP framework. For a point x, a tube of tolerance $m_{\bigcirc}$ is first computed around $h(x)$. Secondly, the inverse map of this interval gives a subset of the 1-D spatial support. Finally, the path-connected component holding x provides the GAN $V^h_{m_{\triangle}}(x)$

Figure 1 gives a visual impression, on a 1-D example, of the computation of a GAN in the LIP framework (i.e. with the $\triangleq$ vector addition (1) and the $\triangle$ vector subtraction (2)).

3.2 Strong GANs

The strong GANs, denoted $N^h_{m_{\bigcirc}}(x)$, are defined as following: $\forall (m_{\bigcirc}, h, x) \in E^{\oplus} \times \mathcal{C} \times D$

$$N^h_{m_{\bigcirc}}(x) = \bigcup_{z \in D} \{V^h_{m_{\bigcirc}}(z) \mid x \in V^h_{m_{\bigcirc}}(z)\} \tag{12}$$

The GANs $V^h_{m_{\bigcirc}}(x)$ do not satisfy the symmetry property contrary to the $N^h_{m_{\bigcirc}}(x)$: $x \in N^h_{m_{\bigcirc}}(y) \Leftrightarrow y \in N^h_{m_{\bigcirc}}(x)$. This symmetry condition is relevant for visual, topological, morphological and practical reasons as explained in [10].

3.3 Illustration

Figure 2 shows the weak and strong GANs of a specific point in a head MR image.

The figure highlights the homogeneity and the correspondence of the GANs with the spatial structures.

3.4 Properties

These sets satisfy several properties as stated in the following.

Let $(m_{\bigcirc}, h, x) \in E^{\oplus} \times \mathcal{C} \times D$

1. reflexivity:

$$x \in V^h_{m_{\bigcirc}}(x) \tag{13}$$

$$x \in N^h_{m_{\bigcirc}}(x) \tag{14}$$

2. increasing with respect to $m_{\bigcirc}$:

$$(m^1_{\bigcirc} \leq m^2_{\bigcirc}) \Rightarrow \begin{pmatrix} V^h_{m^1_{\bigcirc}}(x) \subseteq V^h_{m^2_{\bigcirc}}(x) \\ N^h_{m^1_{\bigcirc}}(x) \subseteq N^h_{m^2_{\bigcirc}}(x) \end{pmatrix} \tag{15}$$

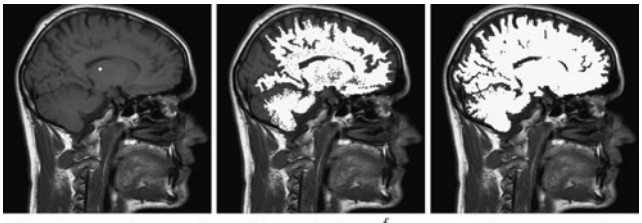

(a) original image f with a seed point x (b) Weak GAN $V^f_{10}(x)$ (c) Strong GAN $N^f_{10}(x)$

Fig. 2 GANs of a selected point in a head MR image (**a**). The GANs are computed in the CLIP framework using the luminance criterion with the homogeneity tolerance value $m = 10$. Image (**b**) (resp. (**c**)) corresponds to the weak GAN (resp. strong GAN) superimposed on the original image

3. equality between iso-valued points:

$$\begin{pmatrix} x \in V^h_{m_{\bigcirc}}(y) \\ h(x) = h(y) \end{pmatrix} \Rightarrow V^h_{m_{\bigcirc}}(x) = V^h_{m_{\bigcirc}}(y) \tag{16}$$

4. $\oplus$-translation invariance:

$$c \in E \Rightarrow \begin{pmatrix} V^{h \oplus c}_{m_{\bigcirc}}(x) = V^h_{m_{\bigcirc}}(x) \\ N^{h \oplus c}_{m_{\bigcirc}}(x) = N^h_{m_{\bigcirc}}(x) \end{pmatrix} \tag{17}$$

5. $\otimes$-multiplication compatibility:

$$\alpha \in \mathbb{R}^+ \backslash \{0\} \Rightarrow \begin{pmatrix} V^{\alpha \otimes h}_{m_{\bigcirc}}(x) = V^h_{\frac{1}{\alpha} \otimes m_{\bigcirc}}(x) \\ N^{\alpha \otimes h}_{m_{\bigcirc}}(x) = N^h_{\frac{1}{\alpha} \otimes m_{\bigcirc}}(x) \end{pmatrix} \tag{18}$$

6. geometric nesting:

$$V^h_{m_{\bigcirc}}(x) \subseteq N^h_{m_{\bigcirc}}(x) \subseteq V^h_{2 \otimes m_{\bigcirc}}(x) \tag{19}$$

7. symmetry:

$$x \in N^h_{m_{\bigcirc}}(y) \Leftrightarrow y \in N^h_{m_{\bigcirc}}(x) \tag{20}$$

The proofs of these properties are given in [11].

The next section introduces two kinds of generalized topologies using the weak and strong GANs. In this way, the underlying pseudoclosure functions will be used for image filtering (Sects. 5 and 6).

4 GAN-Based Pretopologies

4.1 Adaptive Pseudoclosure and Pseudointerior Functions

The weak GANs $V^h_{m_{\bigcirc}}$ and the strong GANs $N^h_{m_{\bigcirc}}$ are extended to subsets of D in the following straightforward way:

$\forall (m_{\bigcirc}, h) \in E^{\oplus} \times \mathcal{C}$

$$\mathrm{V}^h_{m_{\bigcirc}} : \begin{cases} \mathcal{P}(D) \to \mathcal{P}(D) \\ A \mapsto \bigcup_{z \in A} \{V^h_{m_{\bigcirc}}(z)\} \end{cases} \tag{21}$$

$$\mathrm{N}^h_{m_{\bigcirc}} : \begin{cases} \mathcal{P}(D) \to \mathcal{P}(D) \\ A \mapsto \bigcup_{z \in A} \{N^h_{m_{\bigcirc}}(z)\} \end{cases} \tag{22}$$

Naturally, for all x in D, $\mathrm{V}^h_{m_{\bigcirc}}(\{x\}) = V^h_{m_{\bigcirc}}(x)$ and $\mathrm{N}^h_{m_{\bigcirc}}(\{x\}) = N^h_{m_{\bigcirc}}(x)$.

For all $(m_{\bigcirc}, h)$ in $E^{\oplus} \times \mathcal{C}$ both $\mathrm{V}^h_{m_{\bigcirc}}$ and $\mathrm{N}^h_{m_{\bigcirc}}$ define a pseudoclosure function on D. Indeed, the two required properties are satisfied:

1. $\mathrm{V}^h_{m_{\bigcirc}}(\emptyset) = \emptyset$, $\mathrm{N}^h_{m_{\bigcirc}}(\emptyset) = \emptyset$
2. $\forall A \in \mathcal{P}(D)\ A \subseteq \mathrm{V}^h_{m_{\bigcirc}}(A)$, $A \subseteq \mathrm{N}^h_{m_{\bigcirc}}(A)$

The pseudointerior functions $\check{\mathrm{V}}^h_{m_{\bigcirc}}$ and $\check{\mathrm{N}}^h_{m_{\bigcirc}}$, associated to the pseudoclosure functions $\mathrm{V}^h_{m_{\bigcirc}}$ and $\mathrm{N}^h_{m_{\bigcirc}}$, are respectively defined as:

$$\check{\mathrm{V}}^h_{m_{\bigcirc}} : \begin{cases} \mathcal{P}(D) \to \mathcal{P}(D) \\ A \mapsto {}^c(\mathrm{V}^h_{m_{\bigcirc}}({}^cA)) \end{cases} \tag{23}$$

$$\check{\mathrm{N}}^h_{m_{\bigcirc}} : \begin{cases} \mathcal{P}(D) \to \mathcal{P}(D) \\ A \mapsto {}^c(\mathrm{N}^h_{m_{\bigcirc}}({}^cA)) \end{cases} \tag{24}$$

The pseudoclosure functions satisfy several topological axioms, defined in Table 1, as shown in the next subsection.

4.2 Properties of the Adaptive Pseudoclosure Functions

The following properties are meant to hold for all $(m_{\bigcirc}, h, A, B, x, y) \in E^{\oplus} \times \mathcal{C} \times \mathcal{P}(D)^2 \times D^2$:

– axioms systems:

1. $(\mathrm{K}'0) : \begin{cases} \exists A | x \notin \mathrm{V}^h_{m_{\bigcirc}}(A) \\ \exists A | x \notin \mathrm{N}^h_{m_{\bigcirc}}(A) \end{cases}$
2. $(\mathrm{K}0) : \begin{cases} \mathrm{V}^h_{m_{\bigcirc}}(\emptyset) = \emptyset \\ \mathrm{N}^h_{m_{\bigcirc}}(\emptyset) = \emptyset \end{cases}$
3. $(\mathrm{K}1) : A \subseteq B \Rightarrow \begin{cases} \mathrm{V}^h_{m_{\bigcirc}}(A) \subseteq \mathrm{V}^h_{m_{\bigcirc}}(B) \\ \mathrm{N}^h_{m_{\bigcirc}}(A) \subseteq \mathrm{N}^h_{m_{\bigcirc}}(B) \end{cases}$
4. $(\mathrm{KA}) : \begin{cases} \mathrm{V}^h_{m_{\bigcirc}}(D) = D \\ \mathrm{N}^h_{m_{\bigcirc}}(D) = D \end{cases}$
5. $(\mathrm{KB}) : A \cup B = D \Rightarrow \begin{cases} \mathrm{V}^h_{m_{\bigcirc}}(A) \cup \mathrm{V}^h_{m_{\bigcirc}}(B) = D \\ \mathrm{N}^h_{m_{\bigcirc}}(A) \cup \mathrm{N}^h_{m_{\bigcirc}}(B) = D \end{cases}$
6. $(\mathrm{K}2) : \begin{cases} A \subseteq \mathrm{V}^h_{m_{\bigcirc}}(A) \\ A \subseteq \mathrm{N}^h_{m_{\bigcirc}}(A) \end{cases}$
7. $(\mathrm{K}3) : \begin{cases} \mathrm{V}^h_{m_{\bigcirc}}(A \cup B) \subseteq \mathrm{V}^h_{m_{\bigcirc}}(A) \cup \mathrm{V}^h_{m_{\bigcirc}}(B) \\ \mathrm{N}^h_{m_{\bigcirc}}(A \cup B) \subseteq \mathrm{N}^h_{m_{\bigcirc}}(A) \cup \mathrm{N}^h_{m_{\bigcirc}}(B) \end{cases}$

– space comparisons:

$\forall (m_{\bigcirc}{}^1, m_{\bigcirc}{}^2) \in E^{\oplus} \times E^{\oplus}$

$$m_{\bigcirc}{}^1 \leq m_{\bigcirc}{}^2 \Rightarrow \begin{cases} \mathrm{V}^h_{m_{\bigcirc}{}^1}(A) \subseteq \mathrm{V}^h_{m_{\bigcirc}{}^2}(A) \\ \mathrm{N}^h_{m_{\bigcirc}{}^1}(A) \subseteq \mathrm{N}^h_{m_{\bigcirc}{}^2}(A) \end{cases}$$

– translation invariance and scalar multiplication compatibility with respect to h:

1. $c \in E^{\oplus} \Rightarrow \begin{cases} \mathrm{V}^{h \oplus c}_{m_{\bigcirc}}(A) = \mathrm{V}^h_{m_{\bigcirc}}(A) \\ \mathrm{N}^{h \oplus c}_{m_{\bigcirc}}(A) = \mathrm{N}^h_{m_{\bigcirc}}(A) \end{cases}$
2. $\alpha \in \mathbb{R}^+ \backslash \{0\} \Rightarrow \begin{cases} \mathrm{V}^{\alpha \otimes h}_{m_{\bigcirc}}(A) = \mathrm{V}^h_{\frac{1}{\alpha} \otimes m_{\bigcirc}}(A) \\ \mathrm{N}^{\alpha \otimes h}_{m_{\bigcirc}}(A) = \mathrm{N}^h_{\frac{1}{\alpha} \otimes m_{\bigcirc}}(A) \end{cases}$

These properties are direct consequences of the GANs' ones (see (13)–(20)). Note that the axiom (K4) is not satisfied for the proposed GAN-based pseudoclosure functions.

Consequently, $(D, \mathrm{V}^h_{m_{\bigcirc}})$ and $(D, \mathrm{N}^h_{m_{\bigcirc}})$ do not define topological spaces, but pretopological spaces (Table 1).

Those GAN-based pretopological pseudoclosures and pseudointeriors are used in the next section for defining adaptive stack filters.

5 GAN-Based Pretopological Filtering

5.1 Stack Filtering

Stack filters, introduced in [45], are defined by applying a specific boolean operator to each threshold (level) of the gray level image. They constitute a very important class of rank order based filters [14]. They generalize classical filters such as (weighted) median filters, morphological filters ... [15]. The stack filtering principle is first briefly exposed before extending it to the GANIP framework.

A gray level image $f : D \to \tilde{E}$ can be decomposed into its level sets X_t with $t \in \tilde{E}$ (the intensity value range of images):

$$X_t(f) = \{x \in D;\ f(x) \geq t\} \tag{25}$$

The gray level image f can be naturally reconstructed from its level sets:

$$f = \bigvee_t t.\chi_t(f) \tag{26}$$

where χ_t is the indicator function of X_t:

$$\chi_t(f)(x) = \begin{cases} 1 & \text{if } x \in X_t(f) \\ 0 & \text{otherwise} \end{cases}$$

Consider a binary operator ψ acting on the level sets of f, then the stack filtering Ψ of f consists in the following transformation:

$$\Psi(f) = \bigvee_t t.\psi(\chi_t(f))$$

$$\psi(\chi_t(f))(x) = \begin{cases} 1 & \text{if } x \in \psi(X_t(f)) \\ 0 & \text{otherwise} \end{cases} \quad (27)$$

Such filters have to satisfy the stacking property: if the binary output images are piled on top of each other according their threshold level, the result for each point is always a column of 1's with a column of 0's on top. In this way, the output image could be easily and quickly reconstructed. Note that this property is satisfied when ψ is an increasing operator.

Of course, the filter ψ is just a Boolean kernel function operating within a sliding window. It enables to generalize a large class of filters satisfying the threshold decomposition architecture (i.e. filters commuting with any thresholding operation), such as median, max or min filters.

5.2 Classical Pseudoclosure and Pseudointerior Filters

More particularly, those min and max binary operators can be seen as specific pseudoclosures and pseudointeriors functions. Indeed, let define the following operators acting on subsets $A \subseteq D$:

$$\text{clo}_B(A) = A \oplus B = \bigcup \{a + b : a \in A, b \in B\} \quad (28)$$

$$\text{int}_B(A) = A \ominus B = \bigcup \{z : b + z \in A, b \in B\} \quad (29)$$

where $\oplus$ and $\ominus$ denote the Minkowski addition and subtraction respectively, and $B \subset D$ is a sliding neighborhood.

The functions clo_B and int_B define elementary pseudoclosure and pseudointerior functions, respectively (proofs are straightforward). In addition, they are increasing operators (axiom (K1)) so they satisfy the stacking property. In this way, the classical pseudoclosure and pseudointerior filters acting on an image $f \in \mathcal{I}$ are defined as:

$$\text{Clo}_r(f) = \bigvee_t t.\text{clo}_{B_r}(\chi_t(f)) \quad (30)$$

$$\text{Int}_r(f) = \bigvee_t t.\text{int}_{B_r}(\chi_t(f)) \quad (31)$$

where B_r denotes a centered disk of radius r.

Figure 3 shows an illustration of the classical pretopological filters using the pseudointerior int_{B_5} and pseudoclosure clo_{B_5} operators (where B_5 denotes a centered disk of radius 5 pixels) as boolean functions. The filtering is performed on the 'Lena' image.

(a) original image (b) classical pseudointerior filtering (c) classical pseudoclosure filtering

Fig. 3 Classical pretopological filtering using the pseudointerior int_{B_5} and pseudoclosure clo_{B_5} operators (with B_5, a centered disk of radius 5 pixels) as boolean functions

Note that these pseudointerior and pseudoclosure functions correspond respectively to the usual erosion and dilation binary operators defined from mathematical morphology.

More generally, each pseudoclosure function and its associated pseudointerior function satisfying the increasing property (axiom (K1)) define a pretopological filter. Therefore, the GAN-based pretopological pseudoclosure and pseudointerior operators can be introduced as adaptive stack filters.

5.3 Adaptive Pseudoclosure and Pseudointerior Filters

The GAN-based pseudoclosure and pseudointerior are increasing operators (see Sect. 4.2, axiom (K1)). Then, adaptive weak and strong pretopological filters can be defined.

Let $(m_{\hexagon}, h, f) \in E^{\oplus} \times \mathcal{C} \times \mathcal{I}$

$$\text{Clo}\text{V}^h_{m_{\hexagon}}(f) = \bigvee_t t.\text{V}^h_{m_{\hexagon}}(\chi_t(f)) \quad (32)$$

$$\text{Int}\text{V}^h_{m_{\hexagon}}(f) = \bigvee_t t.\check{\text{V}}^h_{m_{\hexagon}}(\chi_t(f)) \quad (33)$$

$$\text{Clo}\text{N}^h_{m_{\hexagon}}(f) = \bigvee_t t.\text{N}^h_{m_{\hexagon}}(\chi_t(f)) \quad (34)$$

$$\text{Int}\text{N}^h_{m_{\hexagon}}(f) = \bigvee_t t.\check{\text{N}}^h_{m_{\hexagon}}(\chi_t(f)) \quad (35)$$

Figure 4 illustrates the adaptive pretopological filtering with both weak and strong GANs.

The strong filters act with more strength than the weak filters. Indeed the weak GANs are included in the strong GANs. This ordering relation implies that

$$f \leq \text{Clo}\text{V}^h_{m_{\hexagon}}(f) \leq \text{Clo}\text{N}^h_{m_{\hexagon}}(f) \quad (36)$$

$$f \geq \text{Int}\text{V}^h_{m_{\hexagon}}(f) \geq \text{Int}\text{N}^h_{m_{\hexagon}}(f) \quad (37)$$

Note that the adaptive weak pretopological filters correspond to specific GAN-based Choquet filters defined in [13]. Also, the adaptive strong pseudoclosure and pseudointerior filters correspond to the GAN-based morphological dilation

(a) original image (b) Adaptive weak pseudointerior filtering (c) Adaptive weak pseudoclosure filtering

(d) Adaptive strong pseudointerior filtering (e) Adaptive strong pseudoclosure filtering

Fig. 4 Adaptive pretopological filtering using the weak and strong pseudointerior and pseudoclosure operators (using the luminance criterion and the homogeneity tolerance value $m = 30$ in the CLIP framework) as boolean functions

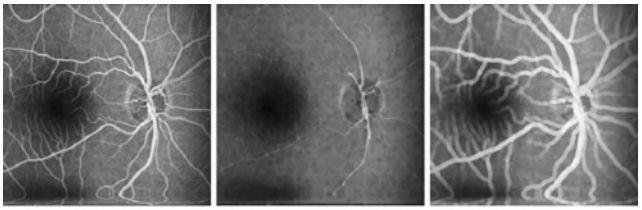

(a) original image (b) Classical pseudointerior filtering (c) Classical pseudoclosure filtering

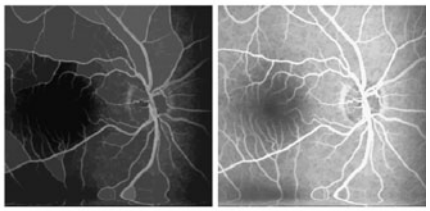

(d) Adaptive strong pseudointerior filtering (e) Adaptive strong pseudoclosure filtering

Fig. 5 Classical pretopological filtering (using the centered disk of radius 3 as sliding window) vs. adaptive pretopological filtering (using the strong GANs computed with the luminance criterion and the homogeneity tolerance value $m = 30$ in the CLIP framework)

and erosion [11, 32], respectively. Therefore, the proposed pretopological filters generalize a large class of GAN-based filters reported in the literature.

5.4 Classical vs. Adaptive Pretopological Filters

The proposed GAN-based pretopological filtering is more efficient than the classical pretopological filtering. Indeed, an image is smoothed while both preserving the transitions and the regions of interest. In particular, this kind of filters could be attractive for image restoration. A comparison of the classical and adaptive pretopological filters is proposed in Fig. 5 where the processing is performed on a human retinal image.

The retinal vessels are rapidly damaged using the classical filtering contrary to the adaptive filters. In addition, no blurring effects occur with the GAN-based filtering.

6 GAN-Based Pretopological Viscous Filtering

One can note in the previous definitions that the classical and adaptive pretopological filters process all level sets identically. On the contrary, viscous operators [25, 27, 44] process the level sets at different scales. It thus enables to define intensity-adaptive operators.

6.1 Classical Viscous Filters

A viscous filter is defined for a gray level image f as:

$$\Phi(f) = \bigvee_t t.\phi_t(\chi_t(f)) \tag{38}$$

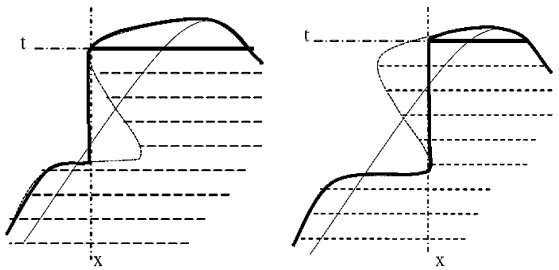

(a) upper envelope (b) lower envelope

Fig. 6 Two stacking schemes for defining viscous filters [43]. *Full line*: initial stack; *dotted line*: filtered stack; *bold line*: final stack reconstruction. x denotes a position within the image spatial support and t a gray level

where $\{\phi_t\}_t$, shortly denoted $\{\phi\}$ can be interpreted as a family of increasing set operators, each operator ϕ_t being assigned to act on the gray level t. If the family $\{\phi\}$ is decreasing, the reconstruction of the different filtered level sets is immediate since the stacking property is satisfied. In the case of a non decreasing family, the reconstruction is performed [43] by considering the lower or upper envelope of the volume formed by the sets (Fig. 6). For example, viscous pseudoclosure (viscous dilation) and viscous pseudointerior (viscous erosion) are defined as [25]:

$$\mathrm{ViscClo}_{\{r\}}(f) = \bigvee_t t.\mathrm{clo}_{B_{r(t)}}(\chi_t(f)) \tag{39}$$

$$\mathrm{ViscInt}_{\{r\}}(f) = \bigvee_t t.\mathrm{int}_{B_{r(t)}}(\chi_t(f)) \tag{40}$$

where $B_{r(t)}$ is a disk of radius $r(t)$, a function of the gray level t. As an example, Fig. 8 shows an illustration of a clas-

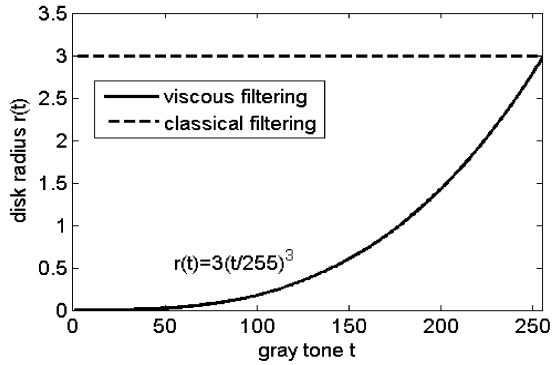

Fig. 7 Disk radius of the sliding window for classical filtering and viscous filtering of a 8-bit image ($M = 256$)

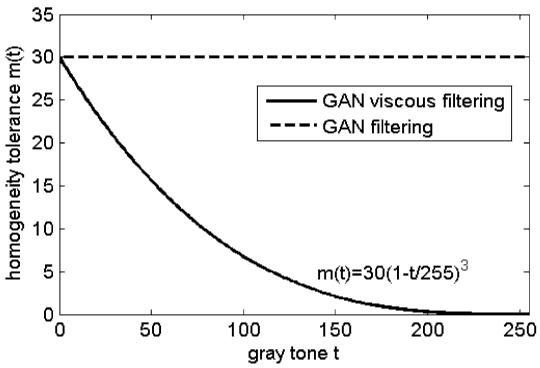

Fig. 9 Homogeneity tolerance of the GANs for adaptive classical filtering and adaptive viscous filtering of a 8-bit image ($M = 256$)

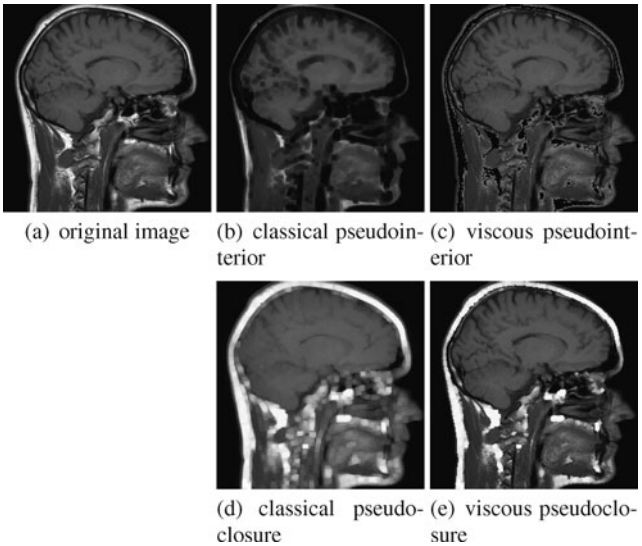

Fig. 8 Classical (**b**, **d**) vs. viscous (**c**, **e**) pseudointerior and pseudoclosure filtering of the original image (**a**) using the function r defined in Fig. 7

sical pseudointerior acting on a 8-bit image ($M = 256$) using a disk or radius 3 vs. a viscous pseudointerior with the function (Fig. 7):

$$r(t) = 3(t/255)^3$$

This function is based on a oil-type model [44]: the viscosity decreases with the gray level. The upper envelope reconstruction is used since the family of viscous pseudoclosures $\{\text{int}_{B_{r(t)}}\}_t$ is not decreasing.

Looking at the resulting images with the choice of the function r, points of highest luminance are strongly eroded while points of lowest luminance are left unchanged.

Nevertheless, those classical viscous filters use fixed-shape isotropic operational windows (which are not adapted to the image itself) and consequently may remove significant image details even if the filtering activity is better controlled than classical filters. The GANIP framework enables to overcome this limitation.

6.2 Adaptive Viscous Filters

Following the viscous notion, GAN-based viscous pretopological filters can be defined in varying the homogeneity tolerance value $m_{\bigcirc}$ of the adaptive pretopological pseudoclosure or pseudointerior.

From a mathematical point of view, the adaptive viscous (weak and strong) pseudoclosure and pseudointerior are then defined as:

$$\text{ViscCloV}^h_{\{m_{\bigcirc}\}}(f) = \bigvee_t t.\text{V}^h_{m_{\bigcirc}(t)}(\chi_t(f)) \tag{41}$$

$$\text{ViscIntV}^h_{\{m_{\bigcirc}\}}(f) = \bigvee_t t.\check{\text{V}}^h_{m_{\bigcirc}(t)}(\chi_t(f)) \tag{42}$$

$$\text{ViscCloN}^h_{\{m_{\bigcirc}\}}(f) = \bigvee_t t.\text{N}^h_{m_{\bigcirc}(t)}(\chi_t(f)) \tag{43}$$

$$\text{ViscIntN}^h_{\{m_{\bigcirc}\}}(f) = \bigvee_t t.\check{\text{N}}^h_{m_{\bigcirc}(t)}(\chi_t(f)) \tag{44}$$

where $m_{\bigcirc}(t)$ is the varying homogeneity tolerance, a function of the gray level t.

As proposed in the classical case, an illustration (Fig. 10) of GAN-based viscous filtering is shown and compared with the GAN-based classical filtering. The filtering process is applied with the weak GANs using the luminance criterion within the CLIP framework. The homogeneity tolerance function for a 8-bit image ($M = 255$), illustrated in Fig. 9, is defined as:

$$m(t) = 30(1 - t/255)^3$$

This function is based on a mercury-type model [44]: the viscosity increases with the gray level.

As previously mentioned, the results first show that images are not damaged by blur using these GAN-based filters.

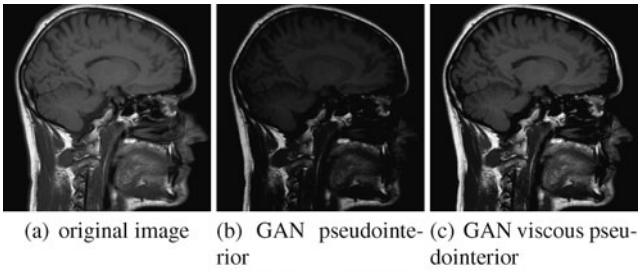

(a) original image (b) GAN pseudointerior (c) GAN viscous pseudointerior

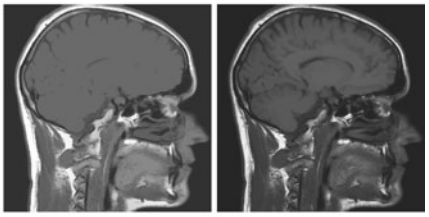

(d) GAN pseudointerior (e) GAN viscous pseudoclosure

Fig. 10 GAN-based classical (**b**, **d**) vs. viscous (**c**, **e**) pseudointerior and pseudointerior filtering of the original image (**a**). The viscous filtering is performed with the function $t \mapsto m(t)$ defined in Fig. 9

In addition, regarding the adaptive viscous filters, the image regions are naturally transformed in accordance with the decreasing function $t \mapsto m(t)$. Points of low luminance are largely transformed compared to those of high luminance. Therefore, the combination of these two characteristics (no blurring effects and controled filtering activity) provide efficient filters for image processing where structures of interest have a specific intensity range.

7 Simulations on Real Application Examples

7.1 Image Restoration

This first application is focused on the restoration of a human brain MR image (Fig. 11). This process is generally required before segmenting the different anatomical structures of the brain. The following GAN pretopological alternating filter, denoted ζ, is both performed in the CLIP and LIP framework in order to compare the two models:

$$\zeta^h_{m_{\bigcirc}}(f) = \mathrm{Clo}\mathrm{N}^h_{m_{\bigcirc}} \circ \mathrm{Int}\mathrm{N}^h_{m_{\bigcirc}}(f) \tag{45}$$

The filtering is applied with the luminance criterion using the homogeneity tolerance value $m_{\bigcirc} = 30$.

This example shows that the filtering in the LIP model mainly acts on low gray level. Indeed, the white structures inside the brain are lesser smoothed than the other structures (with higher gray levels). On the contrary, the filtering in the CLIP model acts on the different gray levels in the same way. This example practically highlights the non linearity of the LIP model and its relevance as shown by Fig. 11.

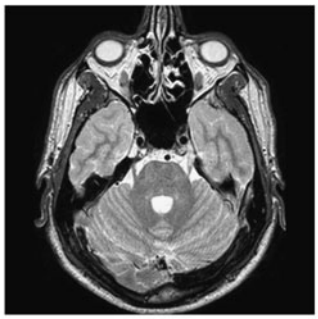

(a) original image

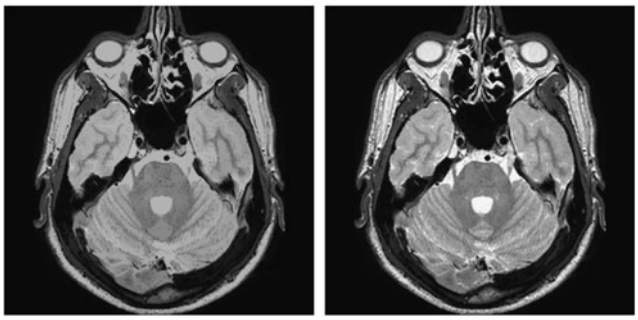

(b) GAN pretopological alternating filtering in the CLIP model (c) GAN pretopological alternating filtering in the LIP model

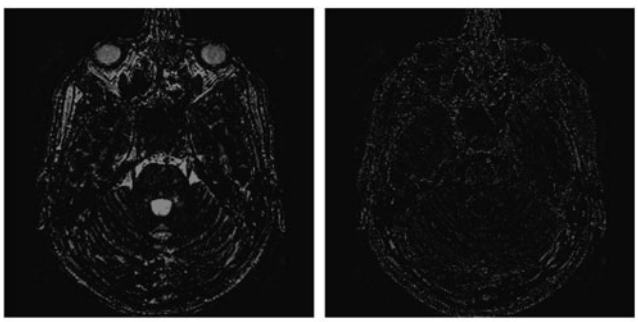

(d) residue of the filtering in the CLIP model (e) residue of the filtering in the LIP model

Fig. 11 Image restoration by a GAN pretopological alternating filtering in the CLIP (**b**) and LIP (**c**) model of a brain MR image (**a**). The residues of the resulting filtered images are shown in (**d**) and (**e**)

7.2 Image Background Subtraction

The second application example concerns the processing of a 8-bit image ($M = 256$) coming from an in-situ cristallisation process of citric acids [34]. The specialists want to get the size and shape distributions of the different cristals. Then, the cristals need to be segmented and characterized. For the segmentation step, a preprocessing is needed such as proposed in [34]. Indeed, the image background is not homogeneous. In this paper, a background subtraction process (Fig. 12) is proposed by applying a GAN-based viscous pseudoclosure filtering using the function: $t \mapsto m(t) = 30 * (t/255)^3$ (oil-type model [44]).

The result shows that the image background is well processed without damaging the size or shape of the cristals.

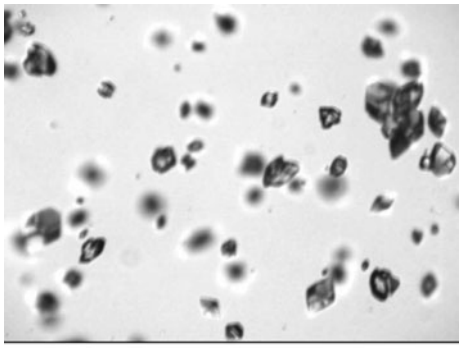

(a) original image

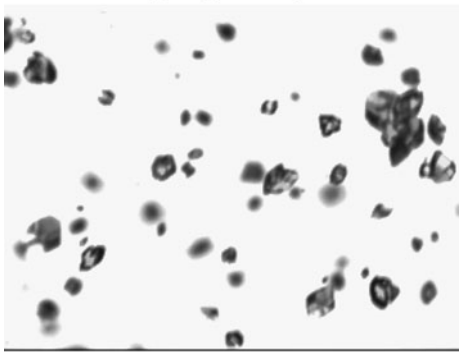

(b) GAN viscous pseudoclosure

Fig. 12 Background subtraction on a cristal image using the GAN-based viscous pseudoclosure filter

Indeed, the filtering activity is specifically focused on image structures of high luminance, i.e. the background. In this way, the cristals could be more easily segmented and then characterized.

7.3 Image Enhancement

Another application of image contrast enhancement is also proposed in Fig. 13 using toggle mappings [26]. A 8-bit image ($M = 256$) of retinal vessels is filtered with a GAN-based viscous toggle mapping using the function $t \mapsto m(t) = 90(t/255)^5$ (oil-type model [44]) in order to enhance the image. From a mathematical point of view, this adaptive toggle mapping is defined as:

$$\kappa^h_{\{m_{\bigcirc}\}}(f)(x) = \begin{cases} \mathrm{ViscCloV}^h_{\{m_{\bigcirc}\}}(f)(x) \\ \quad \text{if } \mathrm{ViscCloV}^h_{\{m_{\bigcirc}\}}(f)(x) - f(x) \\ \qquad < f(x) - \mathrm{ViscIntV}^h_{\{\check{m}_{\bigcirc}\}}(f)(x) \\ \mathrm{ViscIntV}^h_{\{\check{m}_{\bigcirc}\}}(f)(x) \quad \text{otherwise} \end{cases} \tag{46}$$

where $\check{m}_{\bigcirc}(t) = m_{\bigcirc}(M - t)$ (mercury-type model [44]).

This figure shows that retinal vessels (high luminance) become more brighter and background regions of low luminance become more darker. So, the vessels are strongly highlighted compared to the background. In addition, this filter enables to get more homogeneous vessels due to the filtering activity (homogeneity tolerance values). The resulting image is consequently enhanced and suitable for post-processing.

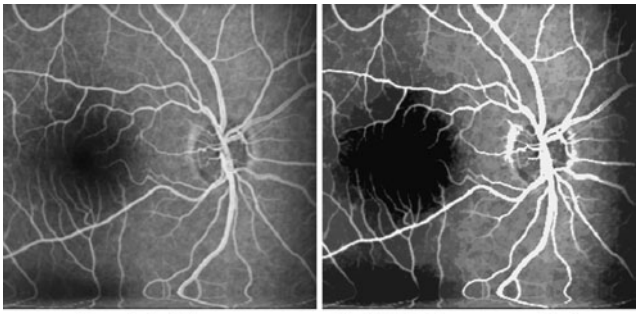

(a) original image (b) GAN viscous pseudoclosure

Fig. 13 Image enhancement of retinal vessels using the GAN-based viscous pseudoclosure filter

8 Conclusion

In this paper, pretopological spaces (generalizing topological ones) have been introduced in the context of the General Adaptive Neighborhood Image Processing (GANIP) approach. These structures have enable efficient adaptive operators to be defined for image processing. The resulting filters process an image while preserving its regions without damaging its transitions. More particularly, GAN-based pretopological filters and GAN-based viscous pretopological filters have been defined and compared through several experiments, giving convincing results. The combination of GAN-based filtering and viscous filtering is particularly efficient in the sense that the filtering is adaptive to the image spatial structures and its activity is controled according to the image gray levels. The theoretical advantages of these adaptive operators have been practically highlighted on real application examples for retoration of MR brain images, background subtraction of cristal images and enhancement of retinal vessel images.

Actually, the authors are working on the Logarithmic Adaptive Neighborhood Image Processing (LANIP) [33] framework for pretopological image filtering.

Acknowledgements The authors would like to thank the Professor P. Gain from the University Hospital Center of Saint-Etienne in France and the Professor G. Fevotte from the LPMG UMR CNRS 5148 in France who have kindly supplied different original images used in this paper.

References

1. Athanaze, Guy: De la théorie des possibilités à la prétopologie et la morphologie mathématique: nouveaux concepts et méthodologies. Ph.D. thesis, INSA, Lyon (2000)

2. Belmandt, Z.: Manuel de prétopologie et ses applications. Hermès, Paris (1993)
3. Bertrand, G.: On topological watersheds. J. Math. Imaging Vis. **22**(2), 217–230 (2005)
4. Bonnevay, S.: Pretopological operators for gray-level image analysis. Studia Inform. Universalis **7**(1), 175–195 (2009)
5. Cech, E.: Topological Spaces. Wiley, New York (1966)
6. Choquet, G.: Topology. Academic Press, San Diego (1966)
7. Couprie, M., Bezerra, F.N., Bertrand, G.: Topological operators for grayscale image processing. J. Electron. Imaging **10**(4), 1003–1015 (2001)
8. Debayle, J., Gavet, Y., Pinoli, J.C.: General adaptive neighborhood image restoration, enhancement and segmentation. In: Lecture Notes in Computer Science, vol. 4141, pp. 29–40. Springer, Berlin (2006)
9. Debayle, J., Pinoli, J.C.: Multiscale image filtering and segmentation by means of adaptive neighborhood mathematical morphology. In: Proceedings of the IEEE International Conference on Image Processing, Genova, Italy, pp. 537–540 (2005)
10. Debayle, J., Pinoli, J.C.: Spatially adaptive morphological image filtering using intrinsic structuring elements. Image Anal. Stereol. **24**(3), 145–158 (2005)
11. Debayle, J., Pinoli, J.C.: General adaptive neighborhood image processing—part I: introduction and theoretical aspects. J. Math. Imaging Vis. **25**(2), 245–266 (2006)
12. Debayle, J., Pinoli, J.C.: General adaptive neighborhood image processing—part II: practical application examples. J. Math. Imaging Vis. **25**(2), 267–284 (2006)
13. Debayle, J., Pinoli, J.C.: General adaptive neighborhood Choquet image filtering. J. Math. Imaging Vis. **35**(3), 173–185 (2009)
14. Fitch, J.P., Coyle, E.J., Gallagher, N.C.: Threshold decomposition of multidimensional ranked order operations. IEEE Trans. Circuits Syst. **32**(5), 445–450 (1985)
15. Hirata, N.S.T.: Stack filters: from definitions to design algorithms. In: Advances in Imaging and Electron Physics, vol. 152, pp. 1–47. Elsevier, Amsterdam (2008)
16. Jourlin, M., Pinoli, J.C.: A model for logarithmic image processing. J. Microsc. **149**, 21–35 (1988)
17. Jourlin, M., Pinoli, J.C.: Logarithmic image processing: the mathematical and physical framework for the representation and processing of transmitted images. Adv. Imaging Electron Phys. **115**, 129–196 (2001)
18. Kong, T.Y., Kopperman, R.: A topological approach to digital topology. Am. Math. Mon. **98**(10), 901–917 (1991)
19. Kong, T.Y., Roscoe, A.W., Rosenfeld, A.: Concepts of digital topology. Topol. Appl. **49**, 219–262 (1992)
20. Kong, T.Y., Rosenfeld, A.: Digital topology: introduction and survey. Comput. Vis. Graph. Image Process. **48**, 357–393 (1989)
21. Kovalevski, V.A.: Finite topology and image analysis. Adv. Electron. Electron Phys. **84**, 197–259 (1992)
22. Kovalevsky, V.A.: Finite topology as applied to image analysis. Comput. Vis. Graph. Image Process. **46**, 141–161 (1989)
23. Largeron, C., Bonnevay, S.: A pretopological approach for structural analysis. Inf. Sci. **144**, 169–185 (2002)
24. Mammass, D., Djeziri, S., Nouboud, F.: A pretopological approach for image segmentation and edge detection. J. Math. Imaging Vis. **15**, 169–179 (2001)
25. Maragos, P., Vachier, C.: A PDE formulation for viscous morphological operators with extensions to intensity-adaptive operators. In: IEEE International Conference on Image Processing, pp. 2200–2203 (2008)
26. Meyer, F., Serra, J.: Contrasts and activity lattices. Signal Process. **16**(4), 303–317 (1989)
27. Meyer, F., Vachier, C.: On the regularization of the watershed transform. In: Advances in Imaging and Electron Physics, vol. 148, pp. 194–249. Elsevier, Amsterdam (2007)
28. Meziane, A., Iftene, T., Selmaoui, N.: Satellite image segmentation by mathematical pretopology and automatic classification. In: SPIE Image Processing, Signal Processing, and Synthetic Aperture Radar for Remote Sensing, pp. 232–236. (1997)
29. Peeters, W.: Semi-pseudometric and pre-topological methods in image analysis. Ph.D. Thesis, Université d'Antwerp, Belgique (1999)
30. Pinoli, J.C.: A general comparative study of the multiplicative homomorphic, log-ratio and logarithmic image processing approaches. Signal Process. **58**, 11–45 (1997)
31. Pinoli, J.C.: The logarithmic image processing model: connections with human brightness perception and contrast estimators. J. Math. Imaging Vis. **7**(4), 341–358 (1997)
32. Pinoli, J.C., Debayle, J.: General adaptive neighborhood mathematical morphology. In: IEEE International Conference on Image Processing, Cairo, Egypt, pp. 2249–2252 (2009)
33. Pinoli, J.C., Debayle, J.: Logarithmic adaptive neighborhood image processing (LANIP): introduction, connections to human brightness perception and application issues. J. Adv. Signal Process., Spec. Issue Image Percept. **2007**, 36105 (2007), 22 p.
34. Presles, B., Debayle, J., Fevotte, G., Pinoli, J.C.: A novel image analysis method for in-situ monitoring the particle size distribution of batch crystallisation process. J. Electron. Imaging **19**(3), 1–7 (2010)
35. Rosenfeld, A.: Digital topology. Am. Math. Mon. **86**, 621–630 (1979)
36. Selmaoui, N., Leschi, C., Emptoz, H.: A new approach to crest lines detection in grey level images. Acta Stereol. **13**(1), 231–236 (1994)
37. Smyth, M.B.: Semi-metrics, closure spaces and digital topology. Theor. Comput. Sci. **151**, 257–276 (1995)
38. Stadler, B.M.R., Stadler, P.F.: Basic Properties of Closure Spaces (2002)
39. Stadler, B.M.R., Stadler, P.F.: Basic Properties of Filter Convergence Spaces (2002)
40. Stadler, B.M.R., Stadler, P.F.: Generalized topological spaces in evolutionary theory and combinatorial chemistry. J. Chem. Inf. Comput. Sci. **42**(3), 577–585 (2002c)
41. Stadler, B.M.R., Stadler, P.F., Shpak, M., Wagner, G.P.: Recombination spaces, metrics, and pretopologies. Z. Phys. Chem. **216**, 217–234 (2002)
42. Tversky, A.: Features of similarity. Psychol. Rev. **84**(4), 327–352 (1977)
43. Vachier, C.: Upper and lower grey-level adaptive morphological operators. In: International Conference on Advances in Pattern Recognition, Kolkata, India, pp. 77–80 (2009)
44. Vachier, C., Meyer, F.: The viscous watershed transform. J. Math. Imaging Vis. **22**(2), 251–267 (2005)
45. Wendt, P.D., Coyle, E.J., Gallagher, N.C.: Stack filters. IEEE Trans. Acoust. Speech Signal Process. **34**(4), 898–911 (1986)

Johan Debayle received his Ph.D. degree in the field of image processing and analysis in 2005. In the beginning of 2006, he joined the French National Institute for Research in Computer Science and Control (INRIA) as a postdoctoral fellow in the field of biomedical image analysis. Since 2007, he is assistant professor in the Laboratory for Image and Pattern Analysis and Modeling within the CIS Center and the LPMG Laboratory, UMR CNRS 5148 at the 'Ecole Nationale Supérieure des Mines de

Saint-Etienne' in France. His research interests include adaptive image processing and morphological analysis.

Jean-Charles Pinoli received Master, Doctorate of Science and 'Habilitation à Diriger des Recherches' degrees in Applied Mathematics in 1983, 1987 and 1992, respectively. From 1985 to 1989, he was member of the opto-electronics department of the Angenieux (Thales) company, Saint-Héand, France, where he pioneered researches in the field of digital imaging and artificial vision. In 1990, he joined the Corporate Research Center of the Pechiney Company, Voreppe, France and was member of the computational technologies department in charge of the imaging activities. Since 2001, he is full professor at the French graduate school 'Ecole Nationale Supérieure des Mines de Saint-Étienne'. He leads the Laboratory for Image and Pattern Analysis and Modeling (LIPAM) within the CIS Center and the LPMG Laboratory, UMR CNRS 5148. His research interests and teaching include Image Processing, Image Analysis, Mathematical Morphology and Computer Vision.